International Journal of Biological Macromolecules 276 (2024) 133822

Contents lists available at ScienceDirect

International Journal of Biological Macromolecules

journal homepage: www.elsevier.com/locate/ijbiomac

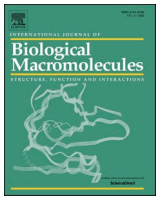

STAG2-RAD21 complex: A unidirectional DNA ratchet mechanism in loop extrusion

David Ros-Pardo, Paulino Gómez-Puertas *, Íñigo Marcos-Alcalde

Centro de Biología Molecular Severo Ochoa, CSIC-UAM, CL Nicolás Cabrera, 1, 28049 Madrid, Spain

ARTICLE INFO

Keywords:
STAG2
RAD21
Loop extrusion
Ratchet mechanism
Martini

ABSTRACT

DNA loop extrusion plays a key role in the regulation of gene expression and the structural arrangement of chromatin. Most existing mechanistic models of loop extrusion depend on some type of ratchet mechanism, which should permit the elongation of loops while preventing their collapse, by enabling DNA to move in only one direction. STAG2 is already known to exert a role as DNA anchor, but the available structural data suggest a possible role in unidirectional DNA motion. In this work, a computational simulation framework was constructed to evaluate whether STAG2 could enforce such unidirectional displacement of a DNA double helix. The results reveal that STAG2 V-shape allows DNA sliding in one direction, but blocks opposite DNA movement via a linear ratchet mechanism. Furthermore, these results suggest that RAD21 binding to STAG2 controls its flexibility by narrowing the opening of its V-shape, which otherwise remains widely open in absence of RAD21. Therefore, in the proposed model, in addition to its already described role as a DNA anchor, the STAG2-RAD21 complex would be part of a ratchet mechanism capable of exerting directional selectivity on DNA sliding during loop extrusion. The identification of the molecular basis of the ratchet mechanism of loop extrusion is a critical step in unraveling new insights into a broad spectrum of chromatin activities and their implications for the mechanisms of chromatin-related diseases.

1. Introduction

From sister chromatid cohesion during replication to regulation of gene expression, DNA repair capabilities and 3D structure management, the cohesin complex is a key element in the administration of the human genome [1–3]. The cohesin complex comprises four core subunits, namely SMC1A/B, SMC3, RAD21, and STAG1/2. Additionally, other associated proteins, including NIPBL, PDS5, and WAPL, play crucial roles in the cohesin complex functions [4–6].

SMC1A/B and SMC3 belong to the SMC (Structural Maintenance of Chromosomes) protein family, a highly conserved group of ATPases. Each SMC protein has an amino- and carboxy-terminal globular domains linked by a central hinge domain through coiled coils. This architectural arrangement forms a rod-like structure, with both globular domains situated on one end and the hinge on the other. The amino-terminal head hosts the Walker A motif, crucial for ATP binding, while the carboxy-terminal head features the Walker B motif and a signature sequence, completing the active site responsible for ATP hydrolysis. The six principal SMC proteins (SMC1–6) engage in specific heterodimeric pairings: SMC1A/B-SMC3 for cohesin, SMC2-SMC4 for condensin, and SMC5-SMC6, each contributing uniquely to the multifaceted functions of the SMC protein family [7,8].

In conjunction with the SMC1A/B-SMC3 proteins, the cohesin complex incorporates the proteins RAD21 (Double-strand-break repair protein rad21 homolog) and STAG1/2 (Stromal antigen 1/2). RAD21, belonging to the kleisin superfamily of proteins, plays a crucial role by binding to the globular heads of both SMC1A/B-SMC3, thereby facilitating the formation of a ring-like structure. Furthermore, RAD21 is instrumental in recruiting STAG1/2 to the complex, contributing to the intricate assembly and functional dynamics of the cohesin machinery [9]. STAG1 and STAG2 are closely homologous proteins with a characteristic HEAT-repeat domain structure, exhibiting variations in their most distal amino- and carboxy-terminal regions. These differences result in diverse but overlapping regulatory roles in gene expression, coupled with unique chromosomal distribution patterns, by which STAG1 is predominantly found in telomeric regions, and STAG2 is more prevalent in centromeric and chromosome arm regions [10–13]. To date, neither of them is known to exert additional functions independent

* Corresponding author.
E-mail address: pagomez@cbm.csic.es (P. Gómez-Puertas).

https://doi.org/10.1016/j.ijbiomac.2024.133822
Received 5 February 2024; Received in revised form 8 July 2024; Accepted 9 July 2024
Available online 14 July 2024

of the cohesin complex.

Consistent with the relevance and variety of its molecular roles, variants in the constituents of the human cohesin complex have been linked to several genetic diseases, most prominently Cornelia de Lange Syndrome [14–16], and cancer [17].

The cohesin complex plays a pivotal role in orchestrating genome expression and maintaining the three-dimensional structure of chromatin through a mechanism known as loop extrusion [3,18,19]. In this process, the complexes bind to specific DNA sites and dynamically translocate along the chromatin fiber, actively forming loops by physically extruding the intervening DNA segments [20,21]. The energy for this process is provided by ATP hydrolysis [22–24]. During interphase, loop extrusion organizes chromatin in TADs (Topologically Associating Domains) which are limited by DNA-bound transcriptional factors CTCF (CCCTC-binding factor) [25,26]. These TADs display an increased probability of intra-domain interactions compared to their surroundings, and they are linked to processes such as gene regulation, DNA replication, recombination, and repair. Importantly, the STAG2-RAD21 complex is acknowledged for its interaction with the N-terminus of CTCFs [27,28].

Over the past few years, several models for loop extrusion have been proposed for SMC complexes [20,29–34].

In the walking model, also known as the tethered-inchworm model, the DNA is tethered to the hinge and to the HAWK (HEAT proteins Associated With Kleisins) subunits, namely NIPBL (Nipped-B-like protein) and STAG1/2, which are, in turn, connected to SMC1A/B and SMC3 head domains. As the heads are linked to the hinge via coiled coils, when they bind to ATP, reaching a closed conformation, they create steric strain between the hinge and themselves. Hydrolysis of the ATP molecules bound by the head domains relieves this steric tension, causing the heads to move apart and pumping the DNA linked to one of the HAWK subunits of the heads into the loop [33].

The pumping model involves trapping a large loop of DNA near the head region. While the heads are bound to ATP, the coiled coils remain open, allowing the formation of a smaller DNA loop between the globular heads and the hinge. Upon ATP hydrolysis, the coiled coils transition into a closed-rod state with the heads juxtaposed, pushing the length of the smaller DNA loop into the larger one, which is still anchored to one of the heads [32].

Similar to the pumping model, in the scrunching model, a large loop is affixed to the globular heads and a smaller loop is formed between the coiled coils. In this case, instead of adopting a closed conformation, the system shifts into a B-shaped conformation. This movement causes the hinge to approach the globular heads by displacing the coiled coils apart, thereby inducing the DNA within the smaller loop to merge into the main loop associated with the heads [35]. In a variation of this model, the coiled coils maintain a rigid rod-like structure, while the hinge translocates to the globular heads through an elbow-like movement of the coiled coils [36–38].

In the Brownian ratchet model, DNA is bound to the two globular heads via NIPBL, and to the hinge via STAG2. In the initial position, often referred to as the “gripping state”, both the hinge with STAG2 and the two globular heads with NIPBL securely immobilize the DNA. In this state, the coiled coils are bent, and the closely-held angle they form keeps the other end of the DNA in place, creating the loop. Following the ATP hydrolysis, the protein enters the “slipping phase”, during which the globular heads open, releasing the DNA. The STAG2-hinge module then draws the DNA into the loop, capitalizing on the tension accumulated in the coiled coils. During this phase STAG2 behaves like a clamp. Subsequently, STAG2 dissociates from the hinge, allowing the cohesin complex to revert to its bent conformation and reassemble into the gripping state [29].

Another proposed mechanism, based on the analysis of alterations in DNA topology induced by condensin, is known as pinch and merge. Resembling the concepts of pumping and scrunching models, in pinch and merge, a small DNA loop is generated and incorporated into an anchored DNA loop [34]. The specific subunits of the condensin complex responsible for this movement remain uncertain.

Despite their different schemes, one thing that all of these models have in common is the need for some mechanism that allows DNA to move in one direction but not in reverse, thus facilitating the formation and elongation of loops and preventing their shortening. The molecular nature of this ratchet-like mechanism remains elusive to this day.

The objectives of this study were: i) to evaluate the role of STAG2 as part of a putative DNA molecular ratchet mechanism, and ii) to examine the influence of RAD21 binding on the flexibility of STAG2.

The results derived from a combination of atomistic and coarse-grained simulations provide support for the hypothesis that the STAG2-RAD21 complex facilitates unidirectional DNA displacement. Additionally, these simulations reveal that RAD21 binding to STAG2 stabilizes a conformation compatible with its role in the proposed ratchet mechanism. Identifying the molecular nature of the ratchet mechanism required by the current loop extrusion models has extensive implications in a wide range of chromatin-related processes.

2. Methods

2.1. Model construction

The STAG2-RAD21-DNA model was built by combining a STAG2-RAD21 model and a 120 bp long DNA model with available structural information on the protein-DNA interaction in *Saccharomyces cerevisiae* homologs.

The STAG2-RAD21 model was built on the Protein Data Bank (PDB) entry 4PJW [39], which already describes the human STAG2-RAD21 complex, the missing gaps of which were modeled through a supervised modeling strategy, combining and curating the predictions obtained using the methods Phyre2 [40] and SwissModel [41].

The 120 bp long CG DNA model was constructed using the x3DNA method [42]. The CG composition was intended to enhance the double strand stability, while the 120 bp length was chosen to prevent border effects during pulling simulations.

To model the STAG2-RAD21 interaction with DNA, the PDB entry 6H8Q [43], was used as reference. 6H8Q provides the 3D structure of the SCC3-SCC1 (Sister chromatid cohesion 3 & 1) complex bound to DNA solved by X-ray crystallography. SCC3 and SCC1 are *Saccharomyces cerevisiae* orthologs to human STAG2 and RAD21 respectively. Thus, the alignment of the STAG2-RAD21 model alpha carbon atoms to those of the protein moiety of the PDB structure 6H8Q, and the alignment of the phosphorus atoms of middle section of the 120 bp DNA model to those of the DNA fragment in the PDB entry 6H8Q, provided an initial mode of interaction between the STAG2-RAD21 model and the 120 bp DNA model. This initial layout was subsequently refined to mimic the protein-DNA interactions observed in the PDB structure 6H8Q, by slightly reorienting the STAG2-RAD21 model to remove the C-terminal clash with the DNA molecules, hence creating an interaction surface between positively charged residues and the DNA double strand analogous to that observed in the PDB entry 6H8Q (Fig. 1A).

Finally, the STAG2 model was obtained by removing the RAD21 moiety of the STAG2-RAD21 model previously described. A general diagram of the modeling process is available at Supplementary Fig. 1A.

2.2. All-atom molecular dynamics simulations

For the all-atom simulations, using the “LEaP” module of Amber Tools [44], the protein moiety of the STAG2-RAD21-DNA model was parameterized with the Amber ff14SB [45] force field, while the Amber OL15 force field [46] was used for the DNA parameterization. The structure was solvated with the “TIP3P” solvent model [47], adding Na^+ and Cl^- ions to neutralize the charge on the system and reach a 150 mM salt concentration [48]. The combination of force fields and solvent models aligns with the Amber manual recommendations.

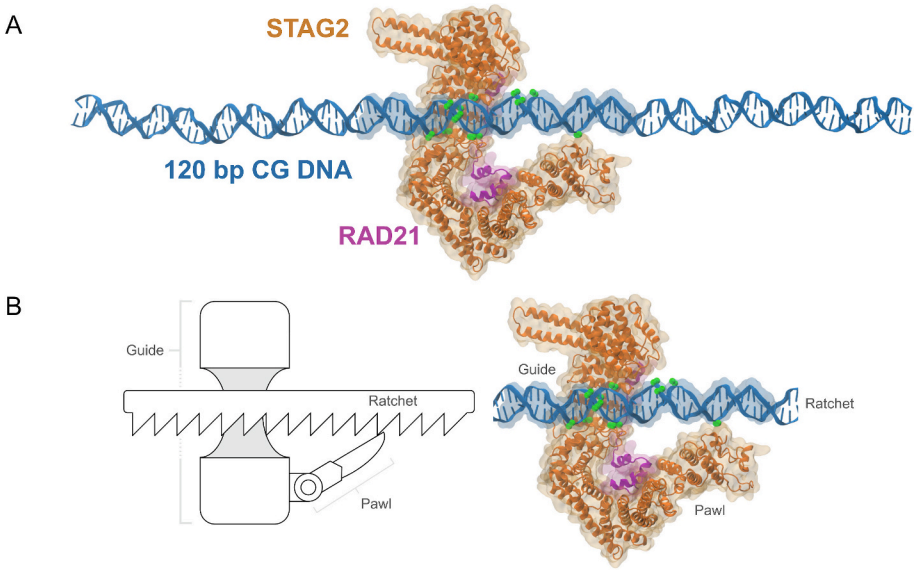

Fig. 1. STAG2-RAD21-DNA model. **A**) 3D structure of the stabilized model constructed for the human STAG2-RAD21 (orange and purple respectively) complex bound to 120 bp of CG DNA (blue). Protein-DNA salt bridges are indicated by green spheres. Semi-transparent volumes indicate the regions used to compute RMSD values. **B**) Components of a linear ratchet mechanism and their translation to the STAG2-RAD21-DNA model. (For interpretation of the references to colour in this figure legend, the reader is referred to the web version of this article.)

Simulations were computed with OpenMM 7.5.1 molecular dynamics simulation toolkit [49]. Tools from the OpenMM suite were used as follows. The non-bonded method used was "Particle Mesh Ewald (PME)" with a non-bonded cutoff of 8 Å. The integrator used was "LangevinMiddleIntegrator" at 298 K with a collision frequency of 1 ps, applying "HBonds" constraints that allowed a time step of 2 fs. To maintain NPT conditions, the pressure coupling was controlled by a "MonteCarloBarostat" at 298 K and 1 bar.

The initial model structure was minimized by the "minimizeEnergy" method with default values. After minimization, a 10 ns long equilibration phase took place, followed by a 2 μs long production phase. To facilitate the removal of modeling clashes in the protein-DNA interfaces, during the minimization and equilibration phases, a positional restraint was applied to the DNA phosphorus atoms while a repulsive quadratic potential was applied to the protein alpha-carbon and DNA phosphorus atoms that were closer than 7 Å. The force constant for both forces was 5 kcal mol^{-1} $Å^{-2}$. These restraints were removed at the end of the equilibration phase.

During the production phase, 4 bp of both ends of the DNA strands were fixed in place by center of mass restraints and by positional restraints. The center of mass restraints allowed the free DNA molecule rotation and were applied during the first 500 ns to facilitate the potential relaxation of the protein-DNA interfaces. The positional restraints did not allow such rotation and were applied during the last 1.5 μs of free MD. In both cases, the force constant applied was 5 kcal mol^{-1} $Å^{-2}$.

The STAG2 and STAG2-RAD21 models, in absence of DNA, were parameterized and simulated in identical conditions to the STAG-RAD21-DNA model, but without requiring any external potentials. The production phase for these conditions was 1 μs long. A general diagram of the simulations produced is available at Supplementary Fig. 1B.

CPPTRAJ 5.1.0 [50] was used for trajectory processing while VMD 1.9.3 [51] was used for visualization and analysis. Parsing and plotting of the measurements produced was performed with Pandas 2.1.1 and Matplotlib 3.8.5 under Python 3.11.5.

2.3. Coarse-grained simulations

The 500 ns frame of the 2 μs long all-atom molecular dynamics (MD) simulation was used to build a coarse-grained model of the STAG-RAD21-DNA complex parameterized with the Martini force field. Bead mapping of the STAG2-RAD21 complex was performed using "martinize2" version 0.7.3 (https://github.com/marrink-lab/vermouth-martinize) with Martini 2.2 [52–54] as the force field. The secondary structure was detected using the algorithm DSSP [55,56], and an elastic network was added. For the DNA component, "martinize-dna.py" script was used with Martini 2.2 DNA [57] force field, specifically the "stiff double strand DNA" type.

The system was solvated in a rectangular water box using "insane.py" [58]. Water beads from the Martini 2.0 solvents force field were used as solvent, while Na^+ and Cl^- beads from the Martini 2.0 ions force field were employed as ions. To prevent water freezing, 10 % of the water beads were converted to anti-freezing water beads using an in-house-designed script. The DNA strand ends were positionally restrained to maintain the stability of the system, with the right end left free in the *Z*-axis to allow the bending of the DNA strand.

Molecular dynamics simulations were performed using GROMACS 2022.5 [59,60], modified with the open-source, community-developed PLUMED library version 2.8.2 [61]. Temperature and pressure coupling were maintained using the "v-rescale" and "c-rescale" algorithms, which achieved greater stability, while constraints were solved using the LINCS algorithm [62]. To further enhance simulation stability, a time step of 0.01 ps was employed. The neighbor search utilized the "Verlet cutoff scheme" with a buffer tolerance of 0.005 kJ mol^{-1} ps^{-1}. Coulomb interactions were managed using the reaction field method with a cutoff of 1.1 nm. A relative dielectric constant of 15 was applied and van der Waals forces were computed with a cutoff of 1.1 nm using a potential-shift with the "Verlet cutoff scheme". The system underwent energy minimization for 50,000 steps using the "steepest descent" algorithm. Equilibration was then carried out for 100,000 steps at 300 K using an NPT (constant Number of particles, constant Pressure, constant Temperature) isothermal-isobaric ensemble.

A 1 μs long free simulation was conducted to relax the STAG2-RAD21-DNA Martini model and assess model stability. The coordinates sampled at 700 ns and 800 ns were used as initial structures for the biased simulations (Fig. 2C).

To study the interaction of the STAG2-RAD21 complex with the DNA, starting from the 800 ns frame of the unbiased trajectory, prospective 2 μs long biased simulations were conducted, applying a

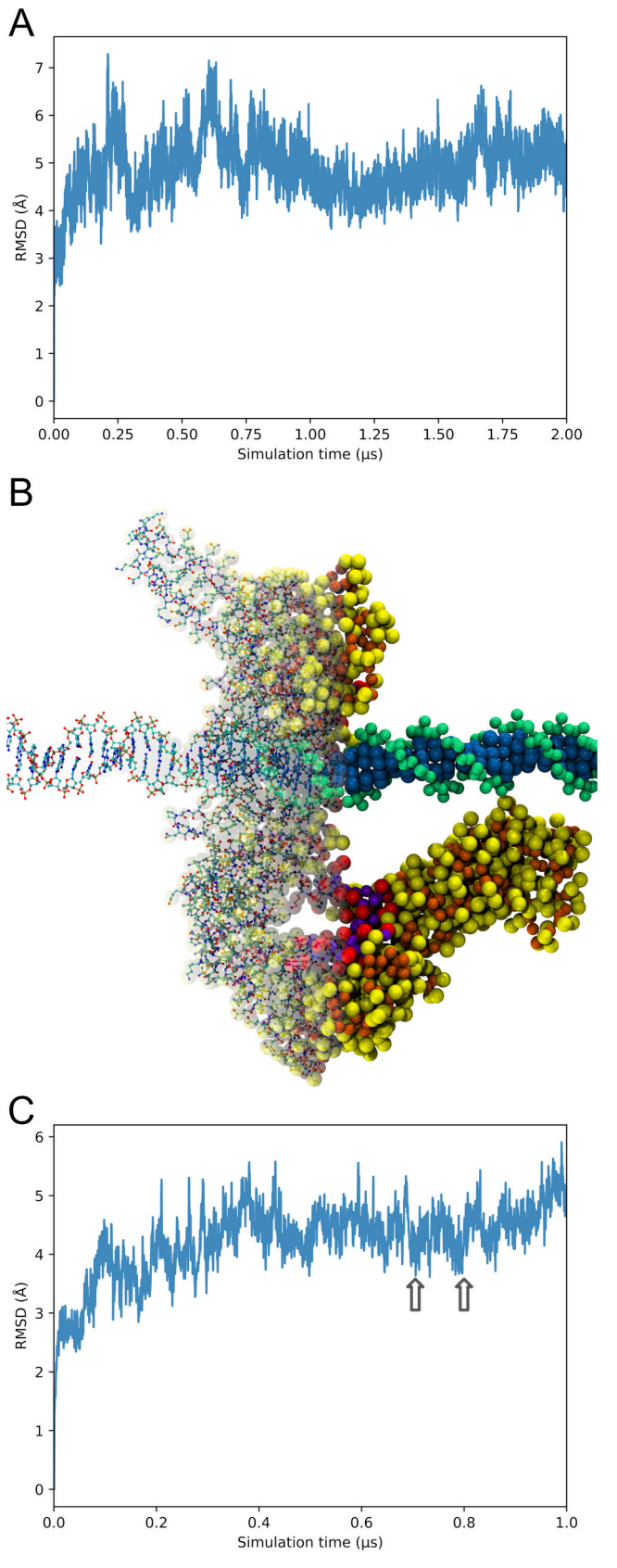

Fig. 2. From atomistic to coarse-grained simulations. **A**) Root Mean Square Deviation (RMSD) of the alpha-carbon trace of the protein and the phosphorus atoms of the DNA region adjacent to the protein moiety calculated for a 2 μs simulation of the atomistic model. **B**) Figure illustrating the process of bead mapping, transforming groups of atoms into individual Martini beads. **C**) Root Mean Square Deviation (RMSD) of the beads mapping to the alpha-carbon trace of the protein and the phosphorus atoms of the DNA region adjacent to the protein moiety, calculated for a 1 μs simulation of the Martini model. The structures utilized for biased simulations are taken from the 700 ns and 800 ns frames (arrows).

constant force to the central region of the protein in contact with the DNA, utilizing the bias module of the PLUMED library. The pulling target was set 43 Å away in each direction along the DNA strand and both ends of the strand were positionally restrained. Increasing force constant (SLOPE) values (5, 6.25, 7.5 and 8.75 kcal mol^{-1} $Å^{-1}$) were tested, each with an RMSD target of 2 Å against the reference structure, until observable movement was detected. Once movement was noticed at 8.75 kcal mol^{-1} $Å^{-1}$, both trajectories (one to the left and one to the right) were extended for 1 μs, reaching a total length of 3 μs each. As duplicate, a second pair of biased trajectories with identical force constant (8.75 kcal mol^{-1} $Å^{-1}$) and total length (3 μs) was computed starting from the 700 ns frame of the unbiased trajectory. Results were visualized using VMD [51] and plots were obtained with Pandas 2.1.1 and Matplotlib 3.8.5 under Python 3.11.5.

To evaluate the conformational effect of RAD21 binding on STAG2 flexibility, STAG2 and STAG2-RAD21 coarse-grained Martini models were constructed and simulated without any biasing potential as previously described, for a total of 1.0 μs.

3. Results

3.1. Generation of a stable STAG2-RAD21-DNA model

Based on the existing structural information of static protein-protein and protein-DNA interactions [39,43], a ratchet mechanism was hypothesized through which STAG2 might influence the direction of DNA movement. This mechanism would require STAG2, RAD21 and a DNA double strand (Fig. 1A). Under these conditions, it was proposed that STAG2 exhibits two regions that act as the guide and pawl elements of the mechanism, while the DNA moiety would play the role of the ratchet (Fig. 1B). To evaluate this hypothesis, a model of the STAG2-RAD21 complex bound to 120 bp of Cytosine-Guanine DNA was built (Fig. 1A).

To allow for structural relaxation and to assess stability, the STAG2-RAD21-DNA model was subjected to 2 μs of MD (Fig. 2A) and the structure sampled at 500 ns was used as template to create a Martini coarse-grained model (Fig. 2B). This coarse-grained model was simulated without biasing potentials for 1 μs, sampling RMSD values consistent with the atomistic model (Fig. 2C).

3.2. STAG2-RAD21 facilitates unidirectional DNA streaming

Once a stable coarse-grained STAG2-RAD21-DNA model was obtained, the frames of the unbiased simulation at 700 ns and 800 ns (Fig. 2C) were extracted to compute duplicates of the biased simulations. In all biased trajectories, while keeping the ends of the DNA molecule fixed, a constant force was applied to the central region of the protein to induce the relative displacement of the STAG2-RAD21 complex along the DNA double strand in each direction (Fig. 3).

In a preliminary phase, starting from the 800 ns unbiased structure, a series of prospective constant force simulations, each with a duration of 2 μs, was performed with increasing force constant values for each direction. The initial force constant was 5 kcal mol^{-1} $Å^{-1}$ and was linearly increased in steps of 1.25 kcal mol^{-1} $Å^{-1}$ for each new simulation until noticeable displacement could be observed in either direction. Force constant values of 5, 6.25, or 7.5 kcal mol^{-1} $Å^{-1}$ failed to induce

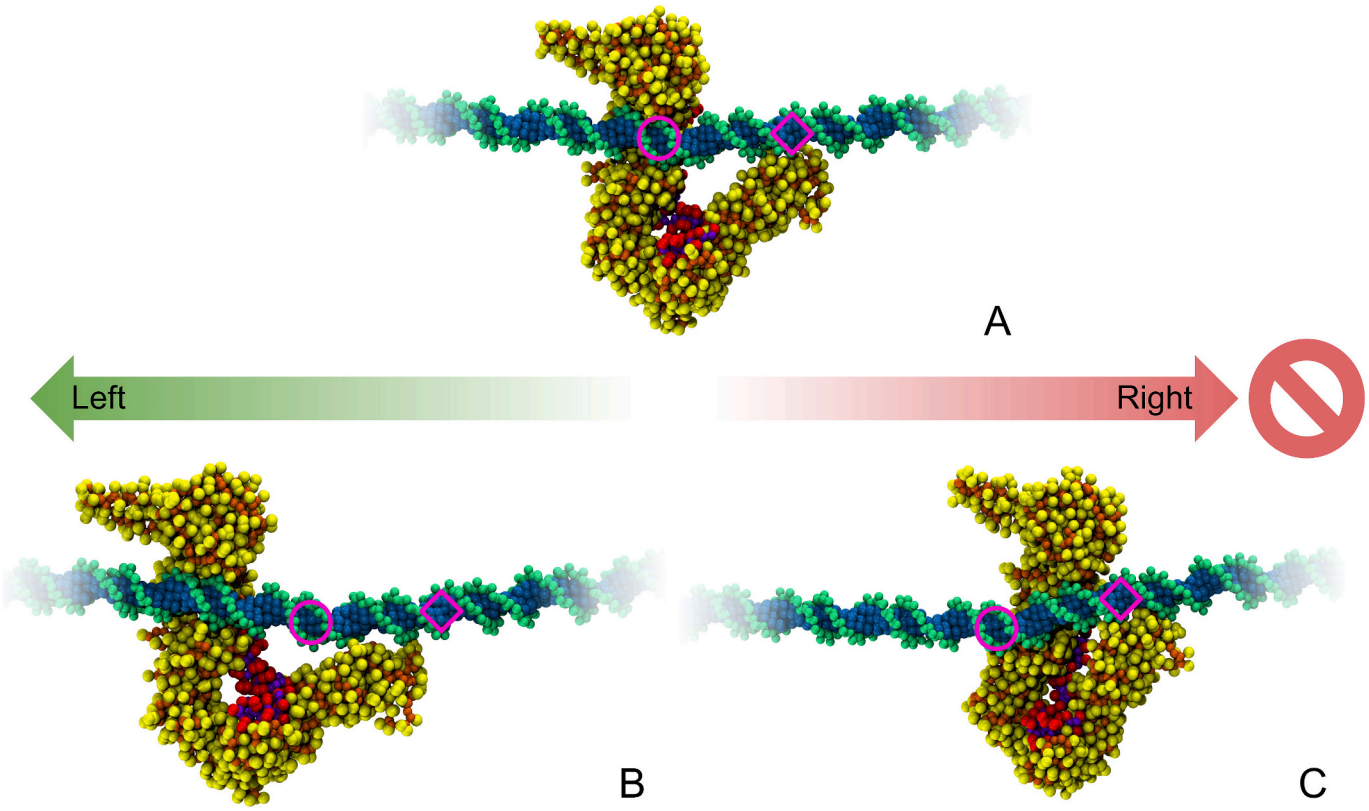

Fig. 3. Pulling setup. General overview of the pulling setup in which, from the same initial simulation frame (**A**), STAG2-RAD21 is pulled to the left (green) and to the right (red). The initial DNA regions interacting with the protein complex are indicated by a purple circle (minor groove) and a purple square (major groove). The final frames of the first pair of constant-force (8.75 kcal mol^{-1} $Å^{-1}$) pulling trajectories to the left (**B**) and to the right (**C**) are shown, indicating the initial protein-DNA interaction regions with the same colored shapes used in panel A. (For interpretation of the references to colour in this figure legend, the reader is referred to the web version of this article.)

significant displacement during the 2 μs simulations. Nevertheless, the 8.75 kcal mol^{-1} $Å^{-1}$ force constant could noticeably displace the STAG2-RAD21 complex and, thus, was established as the constant to be used in subsequent displacement experiments.

For the production phase, the prospective biased simulations with 8.75 kcal mol^{-1} $Å^{-1}$ force constant were then extended for an additional 1 μs to ensure the completion of the displacement motion, reaching a total simulation time of 3 μs. Finally, a duplicate for each pulling direction, starting from the 700 ns unbiased trajectory frame, was obtained using an identical force constant (8.75 kcal mol^{-1} $Å^{-1}$) and total simulation time (3 μs). In total, the production phase yielded four biased trajectories, two pulling to the left and two pulling to the right, starting from two different initial structures.

When the biasing potential was applied to the left, the protein complex moved along the DNA molecule. Fig. 3B shows how the guide region slipped from an initial position in contact with the minor groove of the DNA helix (purple circle in Fig. 3) to the next minor groove, while the pawl region moved equivalently from its initial position in contact with the major groove of the DNA molecule (purple square in Fig. 3) to the next major groove. At the beginning of the movement, a slight opening of the V-shaped structure formed by the STAG2-RAD21 guide and pawl regions was produced by the extension of the pawl region, facilitating its sliding, as would be expected in a linear ratchet mechanism. The final position of the STAG2-RAD21 dimer is equivalent to the initial position, but shifted one full turn to the left, with the protein ready for a new cycle of displacement.

When the biasing potential was applied to the left, the protein complex moved along the DNA molecule. Fig. 3B shows how the guide region slipped from an initial position in contact with the minor groove of the DNA helix (purple circle in Fig. 3) to the next minor groove, while the pawl region moved equivalently from its initial position in contact with the major groove of the DNA molecule (purple square in Fig. 3) to the next major groove. At the beginning of the movement, a slight opening of the V-shaped structure formed by the STAG2-RAD21 guide and pawl regions was produced by the extension of the pawl region, facilitating its sliding, as would be expected in a linear ratchet mechanism. The final position of the STAG2-RAD21 dimer is equivalent to the initial position, but shifted one full turn to the left, with the protein ready for a new cycle of displacement.

In contrast, when force was exerted to the right, the situation was the opposite (Fig. 3C). In this case, the biasing potential was able to partially displace the guide region from the minor groove of the DNA helix (purple circle in Fig. 3) to an intermediate position between the adjacent major and minor grooves. The pawl region, however, remained engaged to the same major groove (purple square in Fig. 3) and was unable to move to the next major groove. As a result, rightward displacement did not occur, and the protein remained stuck in a closed, clamp-like conformation. This situation reveals a clear description of how STAG2-RAD21-DNA constitutes a ratchet mechanism, allowing displacement of the DNA strand only in one direction, blocking the reverse sliding motion. Complete trajectories of the biased simulations in both directions are shown in Supplementary Movie 1 (leftward full-turn displacement) and Supplementary Movie 2 (rightward locked displacement).

Fig. 4 (and Supplementary Table 1) presents a quantification of the movement of the guide and pawl regions relative to their initial position on the DNA strand for both duplicates of each pulling direction. Fig. 4B shows how the guide region is able to move in both directions (left, green-shaded lines; right, red-shaded lines) and in both duplicates, similarly increasing the distance between the protein and its initial position at the DNA minor groove. On the contrary, and as discussed above,

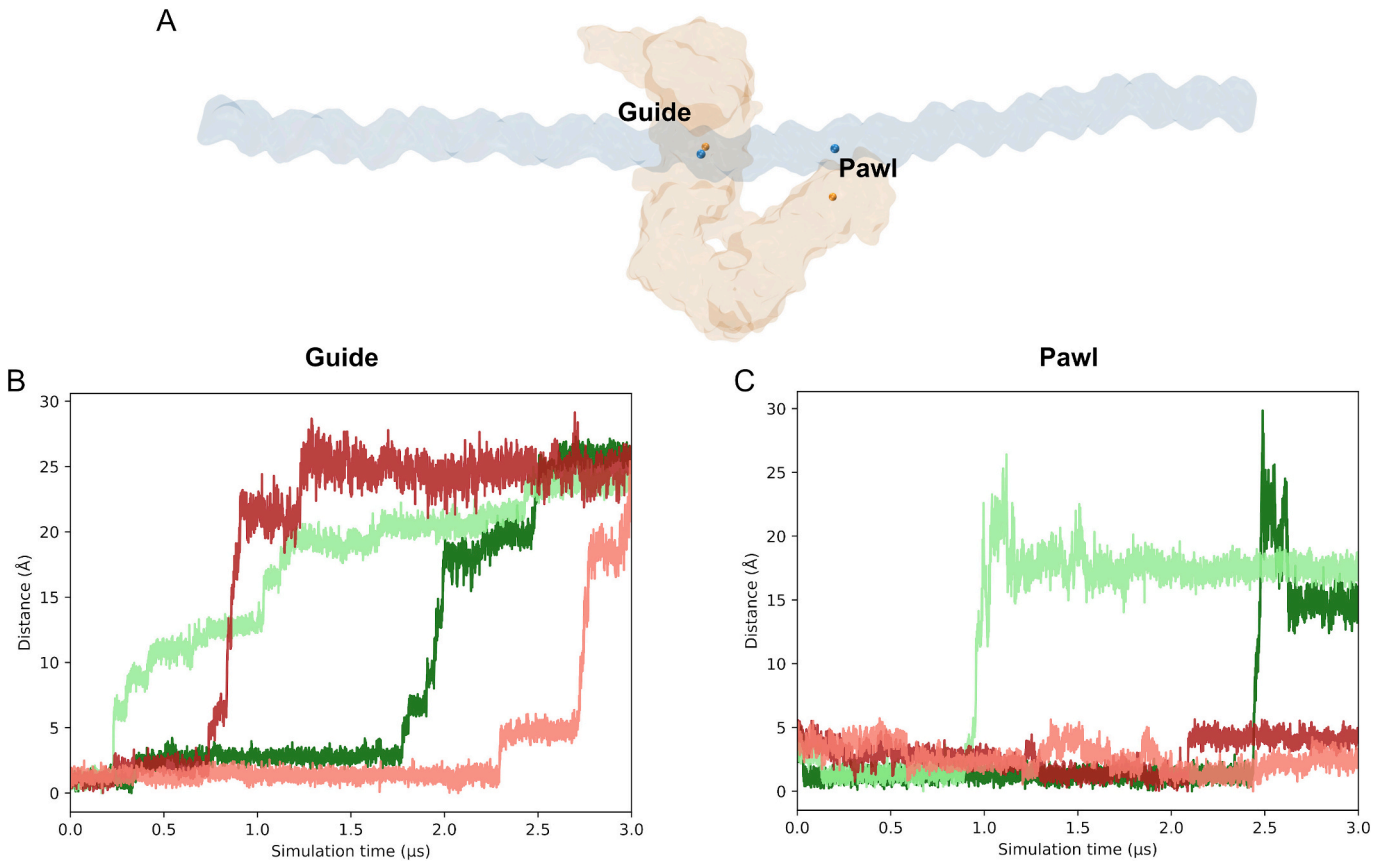

Fig. 4. Distance metrics for the interaction of the guide and pawl regions of STAG2 with the DNA double strand. **A**) Selected reference beads for distance measurements descriptive of the initial interactions between the guide and pawl regions of STAG2 and DNA. Orange spheres indicate STAG2 beads and blue spheres DNA ones. **B**) Evolution of the distance between the STAG2 and DNA beads indicated for the guide region (panel A) for the left-pulling replicas (green) and the right-pulling replicas (red). **C**) Evolution of the distance between the STAG2 and DNA beads indicated in the pawl region (panel A) for the left-pulling replicas (green) and the right-pulling replicas (red). (For interpretation of the references to colour in this figure legend, the reader is referred to the web version of this article.)

the displacement metrics of the pawl in Fig. 4C show that only movement to the left (green-shaded lines) is allowed, while, when the protein is moved to the right (red-shaded lines), its position barely changes, remaining stuck and consequently blocking the displacement of STAG2-RAD21 in that direction. Therefore, the combination of STAG2-RAD21 sliding guide region with a pawl region capable of selectively engaging the DNA "ratchet" grooves depending on the direction of motion, enables a linear ratchet mechanism that allows DNA displacement in a single direction.

3.3. Role of RAD21 in the stabilization of STAG2 closed conformation

In the dynamic model of the STAG2-RAD21 dimer functioning as the protein moiety of the ratchet mechanism shown above, the interactions between DNA and the protein dimer occurred mostly on the surface of the STAG2 protein. Because of this, and reinforced by the fact that the available structures, both for human STAG2 (PDB entry: 4PJW) and its close *S. cerevisiae* homolog SCC3 (PDB entry: 6H8Q), have only been solved interacting with fragments of their respective kleisin subunits (RAD21 and SCC1 respectively), the function of RAD21 in the complex remained to be determined. To study the nature of interaction between the two proteins, a coarse-grained model of the STAG2-RAD21 dimer and a model of STAG2 alone were generated, in the latter case removing the structure corresponding to RAD21. Both models are shown in Fig. 5 (panels 5 A and 5C, respectively).

The two structures were then subjected to a 1 μs long simulation using the Martini force field. In the presence of RAD21 (Fig. 5A), the structure of STAG2 remained virtually unchanged along the simulation (Fig. 5B), maintaining a shape similar to that observed during the DNA displacement experiments shown above. In contrast, when the simulation was performed in the absence of RAD21 (Fig. 5C), the V-shape of the STAG2 structure underwent a remarkable change in the first 200 ns of the simulation and remained in an open conformation until the end of the trajectory (Fig. 5D). This open shape reached by STAG2 in the absence of RAD21 maintained the distance between the guide and pawl regions at very high values, incompatible with the geometry that allows its functional interaction with DNA, and very different from that shown by crystallographic structures [39,43]. For further validation, all-atom simulations of the equivalent models were produced, exhibiting a similar behavior to that observed under coarse-grained conditions (Supplementary Fig. 2).

4. Discussion

In exploring the intricate molecular processes involved in the formation of DNA loops by SMC complexes, several mechanistic models have been proposed over the years, offering diverse perspectives on the complex interplay between SMC complexes and DNA.

In the inchworm model [33], DNA binds to both the hinge and the globular heads through the HAWK subunits, being propelled into the loop through an opening and closing movement of the heads. In the pumping model [32], a large loop is ensnared within the globular heads, with a smaller loop formed between the heads and the hinge. This smaller loop undergoes pumping as the coiled coils shift to a closed rod structure. The scrunching model [35] initially resembles the pumping model, but DNA is pumped by the hinge, displaced by bending the coiled

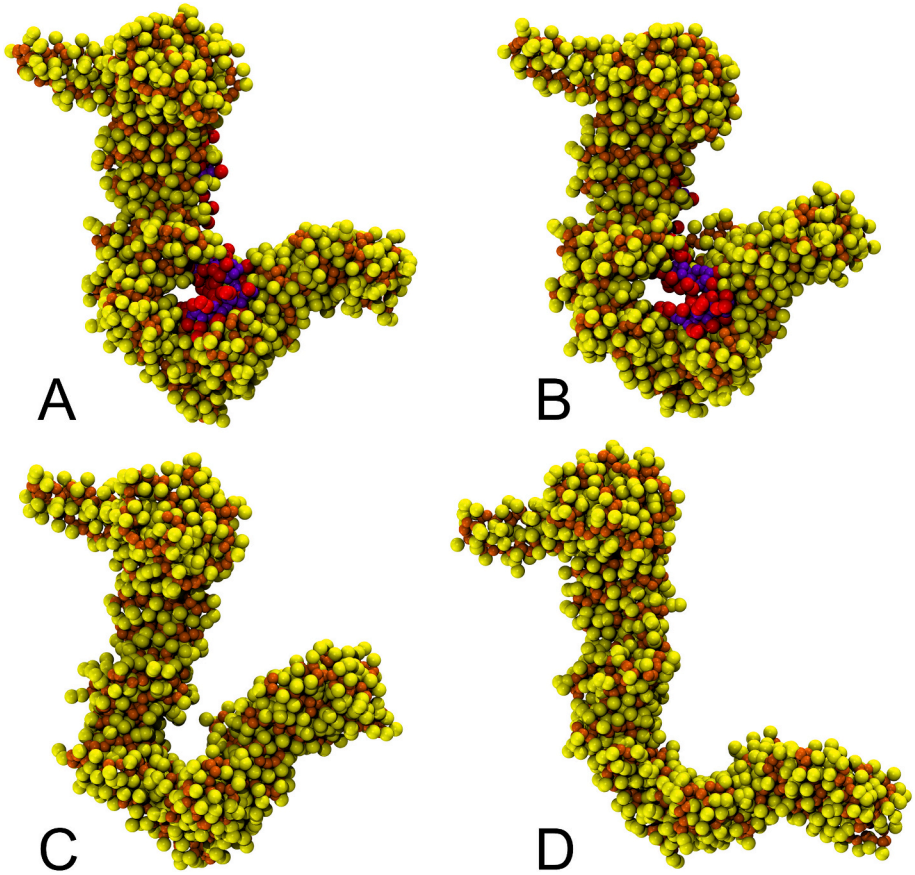

Fig. 5. RAD21 modulates STAG2 flexibility. Results of the coarse-grained simulations of STAG2 without DNA, to assess the effect of RAD21 (purple and red) binding on STAG2 (ochre and yellow) structure. In the upper section, the initial (A) and final (B) frames of the simulation of STAG2 in presence of RAD21 are shown. The lower section illustrates the first (C) and last (D) frames of the simulation in absence of RAD21. (For interpretation of the references to colour in this figure legend, the reader is referred to the web version of this article.)

coils. Lastly, in the brownian ratchet model [29], DNA is initially anchored by the globular heads with NIPBL and the hinge with STAG2, forming a complex with bent coiled coils. The opposite side of the loop traverses the closed angle formed by the bent coiled coils. DNA is drawn into the loop as the globular heads separate, and STAG2 with the hinge pulls the DNA in, utilizing the tension accumulated on the coiled coils.

Once the DNA molecule has moved a distance in the direction appropriate for loop formation, all of the models discussed above rely on a molecular locking mechanism that prevents the DNA from sliding in the opposite direction, thereby reversing the movement and stopping the extrusion process [30]. However, to date, no molecule has been identified that is directly responsible for this mechanism. In the present work, based on dynamic simulations, the STAG1/2-RAD21 complex is proposed to exert a unidirectional restriction on DNA sliding.

STAG1/2 constitute an essential component for cohesin function [63–65], known to mediate DNA anchoring in the cohesin complex [66,67]. The 3D structure of STAG2 in complex with RAD21 has been solved by X-ray crystallography at high resolutions [39,66], enabling the generation of high-quality models. According to the simulation results, in which the STAG2-RAD21 complex is constrained to move in only one direction (Fig. 3), it was proposed that STAG2 serves a dual role. Beyond its established function as an anchor for cohesin complex DNA binding, it would also act as a safety mechanism, effectively preventing DNA from reversing its trajectory during the molecular motions of the cohesin complex associated with loop extrusion. This proposed ratchet mechanism would solely be the product of the structural constraints imposed by STAG2-RAD21 geometry when interacting with the DNA strand. Furthermore, the close homology relationship between STAG1/2/3 proteins suggests that this ratchet function might be a common feature among them. Nevertheless, extending these results to STAG1/3 remains a task for future research.

In addition, the trajectories used to explore the directionality selection of DNA displacement by STAG2 revealed an instrumental role of STAG2 flexibility, and its association to RAD21, in maintaining the functional shape of the STAG2-RAD21 complex.

The RAD21 moiety bound to STAG2 in the available structural data, is located at a V-shaped region of STAG2 (Fig. 1A) that is opened when DNA sliding is allowed and closed when it is blocked. These results suggest that the presence of RAD21 modifies the rest position of STAG2 V-shaped region, being similar to the crystallographic DNA-bound conformation when RAD21 is present (Fig. 5B), and much more open when it is not (Fig. 5D).

The main limitations of this study are that the proposed ratchet model and STAG2/RAD21 interactions are based on computational molecular dynamics simulations and homology models. In the future, experimental validation, such as single molecule studies, electron microscopy or chromosome conformation capture techniques, will be needed to assess the validity of the proposed theories and to test their implications in genome expression regulation and chromatin 3D structure management, as well as their potential repercussions in the rationalization of disease-causing variants. In addition, future computational work involving more proteins of the complex in the simulation system, as well as the study of homologous systems and their functional similarities and differences, will allow to broaden the knowledge of this area of study.

In conclusion, these results support that STAG2 could exert a molecular ratchet role in loop extrusion, a general requirement for most of the proposed extrusion mechanism models that remain unresolved to

date. This ratchet mechanism would allow DNA loop extension in one direction, while preventing loop collapse in the opposite one. The STAG2-RAD21 complex could therefore be the system that drives the unidirectionality of DNA displacement in loop extrusion.

Supplementary data to this article can be found online at https://doi.org/10.1016/j.ijbiomac.2024.133822.

Funding

This research was financed by the following grants: Ministerio de Ciencia, Innovación y Universidades, Agencia Estatal de Investigación (MCIU-AEI, RTI2018-094434-B-I00 and PID2021-126625OB-I00/10.13039/501100011033/FEDER, EU) and Instituto de Salud Carlos III (DTS20-00024).

CRediT authorship contribution statement

David Ros-Pardo: Writing – review & editing, Writing – original draft, Methodology, Investigation, Formal analysis, Conceptualization. **Paulino Gómez-Puertas:** Writing – review & editing, Writing – original draft, Supervision, Formal analysis, Conceptualization. **Íñigo Marcos-Alcalde:** Writing – review & editing, Writing – original draft, Supervision, Methodology, Investigation, Formal analysis, Conceptualization.

Declaration of competing interest

No competing interest is declared.

Data availability

The data analyzed during this study are included in this published article. Additional supporting data are available from the corresponding authors upon reasonable request.

Acknowledgments

The computational support of the “Centro de Computación Científica CCC-UAM” is gratefully recognized.

References

[1] T. Gligoris, J. Löwe, Structural insights into ring formation of cohesin and related Smc complexes, Trends Cell Biol. 26 (2016) 680–693, https://doi.org/10.1016/j.tcb.2016.04.002.
[2] J.-M. Peters, A. Tedeschi, J. Schmitz, The cohesin complex and its roles in chromosome biology, Genes Dev. 22 (2008) 3089–3114, https://doi.org/10.1101/gad.1724308.
[3] J.A. Horsfield, Full circle: a brief history of cohesin and the regulation of gene expression, FEBS J. 290 (2022) 1670–1687, https://doi.org/10.1111/febs.16362.
[4] D. Alonso-Gil, A. Losada, NIPBL and cohesin: new take on a classic tale, Trends Cell Biol. 33 (2023) 860–871, https://doi.org/10.1016/j.tcb.2023.03.006.
[5] R.V. Skibbens, Condensins and cohesins - one of these things is not like the other!, J. Cell Sci. 132 (2019) jcs220491, https://doi.org/10.1242/jcs.220491.
[6] G. Wutz, C. Várnai, K. Nagasaka, D.A. Cisneros, R.R. Stocsits, W. Tang, S. Schoenfelder, G. Jessberger, M. Muhar, M.J. Hossain, N. Walther, B. Koch, M. Kueblbeck, J. Ellenberg, J. Zuber, P. Fraser, J.-M. Peters, Topologically associating domains and chromatin loops depend on cohesin and are regulated by CTCF, WAPL, and PDS5 proteins, EMBO J. 36 (2017) 3573–3599, https://doi.org/10.15252/embj.201798004.
[7] S.H. Harvey, M.J. Krien, M.J. O'Connell, Structural maintenance of chromosomes (SMC) proteins, a family of conserved ATPases, Genome Biol. 3 (2002), https://doi.org/10.1186/gb-2002-3-2-reviews3003 reviews3003.1.
[8] E. Kim, R. Barth, C. Dekker, Looping the genome with SMC complexes, Annu. Rev. Biochem. 92 (2023) 15–41, https://doi.org/10.1146/annurev-biochem-032620-110506.
[9] H. Cheng, N. Zhang, D. Pati, Cohesin subunit RAD21: from biology to disease, Gene 758 (2020) 144966, https://doi.org/10.1016/j.gene.2020.144966.
[10] A. Cuadrado, A. Losada, Specialized functions of cohesins STAG1 and STAG2 in 3D genome architecture, Curr. Opin. Genet. Dev. 61 (2020) 9–16, https://doi.org/10.1016/j.gde.2020.02.024.
[11] N.L. Arruda, Z.M. Carico, M. Justice, Y.F. Liu, J. Zhou, H.C. Stefan, J.M. Dowen, Distinct and overlapping roles of STAG1 and STAG2 in cohesin localization and gene expression in embryonic stem cells, Epigenetics Chromatin 13 (2020), https://doi.org/10.1186/s13072-020-00353-9.
[12] N. Zhang, Y. Jiang, Q. Mao, B. Demeler, Y.J. Tao, D. Pati, Characterization of the interaction between the cohesin subunits Rad21 and SA1/2, PLoS One 8 (2013) e69458, https://doi.org/10.1371/journal.pone.0069458.
[13] S. Canudas, S. Smith, Differential regulation of telomere and centromere cohesion by the Scc3 homologues SA1 and SA2, respectively, in human cells, J. Cell Biol. 187 (2009) 165–173, https://doi.org/10.1083/jcb.200903096.
[14] J. Pié, B. Puisac, M. Hernández-Marcos, M.E. Teresa-Rodrigo, M. Gil-Rodríguez, C. Baquero-Montoya, M. Ramos-Cáceres, M. Bernal, A. Ayerza-Casas, I. Bueno, P. Gómez-Puertas, F.J. Ramos, Special cases in Cornelia de Lange syndrome: the Spanish experience, Am. J. Med. Genet. C: Semin. Med. Genet. 172 (2016) 198–205, https://doi.org/10.1002/ajmg.c.31501.
[15] M. Kaur, J. Blair, B. Devkota, S. Fortunato, D. Clark, A. Lawrence, J. Kim, W. Do, B. Semeo, O. Katz, D. Mehta, N. Yamamoto, E. Schindler, Z. Al Rawi, N. Wallace, J. J. Wilde, J. McCallum, J. Liu, D. Xu, M. Jackson, S. Rentas, A.A. Tayoun, Z. Zhe, O. Abdul-Rahman, B. Allen, M.A. Angula, K. Anyane-Yeboa, J. Argente, P.H. Arn, L. Armstrong, L. Basel-Salmon, G. Baynam, L.M. Bird, D. Bruegger, G.-S. Ch'ng, D. Chitayat, R. Clark, G.F. Cox, U. Dave, E. DeBaere, M. Field, J.M. Graham, K. W. Gripp, R. Greenstein, N. Gupta, R. Heidenreich, J. Hoffman, R.J. Hopkin, K. L. Jones, M.C. Jones, A. Kariminejad, J. Kogan, B. Lace, J. Leroy, S.A. Lynch, M. McDonald, K. Meagher, N. Mendelsohn, I. Micule, J. Moeschler, S. Nampoothiri, K. Ohashi, C.M. Powell, S. Ramanathan, S. Raskin, E. Roeder, M. Rio, A.F. Rope, K. Sangha, A.E. Scheuerle, A. Schneider, S. Shalev, V. Siu, R. Smith, C. Stevens, T. Tkemaladze, J. Toimie, H. Toriello, A. Turner, P.G. Wheeler, S.M. White, T. Young, K.M. Loomes, M. Pipan, A.T. Harrington, E. Zackai, R. Rajagopalan, L. Conlin, M.A. Deardorff, D. McEldrew, J. Pie, F. Ramos, A. Musio, A.D. Kline, K. Izumi, S.E. Raible, I.D. Krantz, Genomic analyses in Cornelia de Lange Syndrome and related diagnoses: Novel candidate genes, genotype-phenotype correlations and common mechanisms, Am. J. Med. Genet. A 191 (2023) 2113–2131, https://doi.org/10.1002/ajmg.a.63247.
[16] D. Ros-Pardo, P. Gómez-Puertas, Í. Marcos-Alcalde, STAG2: computational analysis of missense variants involved in disease, Int. J. Mol. Sci. 25 (2024) 1280, https://doi.org/10.3390/ijms25021280.
[17] M. Di Nardo, M.M. Pallotta, A. Musio, The multifaceted roles of cohesin in cancer, J. Exp. Clin. Cancer Res. 41 (2022), https://doi.org/10.1186/s13046-022-02321-5.
[18] C. Perea-Resa, L. Wattendorf, S. Marzouk, M.D. Blower, Cohesin: behind dynamic genome topology and gene expression reprogramming, Trends Cell Biol. 31 (2021) 760–773, https://doi.org/10.1016/j.tcb.2021.03.005.
[19] H. Shin, Y. Kim, Regulation of loop extrusion on the interphase genome, Crit. Rev. Biochem. Mol. Biol. 58 (2023) 1–18, https://doi.org/10.1080/10409238.2023.2182273.
[20] I.F. Davidson, J.-M. Peters, Genome folding through loop extrusion by SMC complexes, Nat. Rev. Mol. Cell Biol. 22 (2021) 445–464, https://doi.org/10.1038/s41580-021-00349-7.
[21] C. Hoencamp, B.D. Rowland, Genome control by SMC complexes, Nat. Rev. Mol. Cell Biol. 24 (2023) 633–650, https://doi.org/10.1038/s41580-023-00609-8.
[22] E.J. Banigan, L.A. Mirny, Loop extrusion: theory meets single-molecule experiments, Curr. Opin. Cell Biol. 64 (2020) 124–138, https://doi.org/10.1016/j.ceb.2020.04.011.
[23] Í. Marcos-Alcalde, J.I. Mendieta-Moreno, B. Puisac, M.C. Gil-Rodríguez, M. Hernández-Marcos, D. Soler-Polo, F.J. Ramos, J. Ortega, J. Pié, J. Mendieta, P. Gómez-Puertas, Two-step ATP-driven opening of cohesin head, Sci. Rep. 7 (2017) 3266, https://doi.org/10.1038/s41598-017-03118-9.
[24] Y. Kim, Z. Shi, H. Zhang, I.J. Finkelstein, H. Yu, Human cohesin compacts DNA by loop extrusion, Science 366 (2019) 1345–1349, https://doi.org/10.1126/science.aaz4475.
[25] J.A. da Costa-Nunes, D. Noordermeer, TADs: dynamic structures to create stable regulatory functions, Curr. Opin. Struct. Biol. 81 (2023) 102622, https://doi.org/10.1016/j.sbi.2023.102622.
[26] G.A. Busslinger, R.R. Stocsits, P. van der Lelij, E. Axelsson, A. Tedeschi, N. Galjart, J.-M. Peters, Cohesin is positioned in mammalian genomes by transcription, CTCF and Wapl, Nature 544 (2017) 503–507, https://doi.org/10.1038/nature22063.
[27] E.P. Nora, L. Caccianini, G. Fudenberg, K. So, V. Kameswaran, A. Nagle, A. Uebersohn, B. Hajj, A.L. Saux, A. Coulon, L.A. Mirny, K.S. Pollard, M. Dahan, B. G. Bruneau, Molecular basis of CTCF binding polarity in genome folding, Nat. Commun. 11 (2020), https://doi.org/10.1038/s41467-020-19283-x.
[28] Y. Li, J.H.I. Haarhuis, Á. Sedeño Cacciatore, R. Oldenkamp, M.S. van Ruiten, L. Willems, H. Teunissen, K.W. Muir, E. de Wit, B.D. Rowland, D. Panne, The structural basis for cohesin-CTCF-anchored loops, Nature 578 (2020) 472–476, https://doi.org/10.1038/s41586-019-1910-z.
[29] T.L. Higashi, G. Pobegalov, M. Tang, M.I. Molodtsov, F. Uhlmann, A Brownian ratchet model for DNA loop extrusion by the cohesin complex, eLife 10 (2021), https://doi.org/10.7554/elife.67530.
[30] S. Datta, L. Lecomte, C.H. Haering, Structural insights into DNA loop extrusion by SMC protein complexes, Curr. Opin. Struct. Biol. 65 (2020) 102–109, https://doi.org/10.1016/j.sbi.2020.06.009.
[31] E. Kabirova, A. Nurislamov, A. Shadskiy, A. Smirnov, A. Popov, P. Salnikov, N. Battulin, V. Fishman, Function and evolution of the loop extrusion machinery in animals, Int. J. Mol. Sci. 24 (2023) 5017, https://doi.org/10.3390/ijms24055017.
[32] J.F. Marko, P. De Los Rios, A. Barducci, S. Gruber, DNA-segment-capture model for loop extrusion by structural maintenance of chromosome (SMC) protein complexes, Nucleic Acids Res. 47 (2019) 6956–6972, https://doi.org/10.1093/nar/gkz497.

[33] M.H. Nichols, V.G. Corces, A tethered-inchworm model of SMC DNA translocation, Nat. Struct. Mol. Biol. 25 (2018) 906–910, https://doi.org/10.1038/s41594-018-0135-4.
[34] B. Martínez-García, S. Dyson, J. Segura, A. Ayats, E.E. Cutts, P. Gutierrez-Escribano, L. Aragón, J. Roca, Condensin pinches a short negatively supercoiled DNA loop during each round of ATP usage, EMBO J. 42 (2022), https://doi.org/10.15252/embj.2022111913.
[35] J.-K. Ryu, A.J. Katan, E.O. van der Sluis, T. Wisse, R. de Groot, C.H. Haering, C. Dekker, The condensin holocomplex cycles dynamically between open and collapsed states, Nat. Struct. Mol. Biol. 27 (2020) 1134–1141, https://doi.org/10.1038/s41594-020-0508-3.
[36] Y.-M. Soh, F. Bürmann, H.-C. Shin, T. Oda, K.S. Jin, C.P. Toseland, C. Kim, H. Lee, S.J. Kim, M.-S. Kong, M.-L. Durand-Diebold, Y.-G. Kim, H.M. Kim, N.K. Lee, M. Sato, B.-H. Oh, S. Gruber, Molecular basis for SMC rod formation and its dissolution upon DNA binding, Mol. Cell 57 (2015) 290–303, https://doi.org/10.1016/j.molcel.2014.11.023.
[37] F. Bürmann, B.-G. Lee, T. Than, L. Sinn, F.J. O'Reilly, S. Yatskevich, J. Rappsilber, B. Hu, K. Nasmyth, J. Löwe, A folded conformation of MukBEF and cohesin, Nat. Struct. Mol. Biol. 26 (2019) 227–236, https://doi.org/10.1038/s41594-019-0196-z.
[38] M.T. Hons, P.J. Huis in 't Veld, J. Kaesler, P. Rombaut, A. Schleiffer, F. Herzog, H. Stark, J.-M. Peters, Topology and structure of an engineered human cohesin complex bound to Pds5B, Nat. Commun. 7 (2016), https://doi.org/10.1038/ncomms12523.
[39] K. Hara, G. Zheng, Q. Qu, H. Liu, Z. Ouyang, Z. Chen, D.R. Tomchick, H. Yu, Structure of cohesin subcomplex pinpoints direct shugoshin-Wapl antagonism in centromeric cohesion, Nat. Struct. Mol. Biol. 21 (2014) 864–870, https://doi.org/10.1038/nsmb.2880.
[40] L.A. Kelley, S. Mezulis, C.M. Yates, M.N. Wass, M.J.E. Sternberg, The Phyre2 web portal for protein modeling, prediction and analysis, Nat. Protoc. 10 (2015) 845–858, https://doi.org/10.1038/nprot.2015.053.
[41] A. Waterhouse, M. Bertoni, S. Bienert, G. Studer, G. Tauriello, R. Gumienny, F. T. Heer, T.A.P. de Beer, C. Rempfer, L. Bordoli, R. Lepore, T. Schwede, SWISS-MODEL: homology modelling of protein structures and complexes, Nucleic Acids Res. 46 (2018) W296–W303, https://doi.org/10.1093/nar/gky427.
[42] A.V. Colasanti, X.-J. Lu, W.K. Olson, Analyzing and building nucleic acid structures with 3DNA, J. Vis. Exp. (2013) e4401, https://doi.org/10.3791/4401.
[43] Y. Li, K.W. Muir, M.W. Bowler, J. Metz, C.H. Haering, D. Panne, Structural basis for Scc3-dependent cohesin recruitment to chromatin, Elife 7 (2018) e38356, https://doi.org/10.7554/eLife.38356.
[44] D.A. Case, H.M. Aktulga, K. Belfon, D.S. Cerutti, G.A. Cisneros, V.W.D. Cruzeiro, N. Forouzesh, T.J. Giese, A.W. Götz, H. Gohlke, S. Izadi, K. Kasavajhala, M. C. Kaymak, E. King, T. Kurtzman, T.-S. Lee, P. Li, J. Liu, T. Luchko, R. Luo, M. Manathunga, M.R. Machado, H.M. Nguyen, K.A. O'Hearn, A.V. Onufriev, F. Pan, S. Pantano, R. Qi, A. Rahnamoun, A. Risheh, S. Schott-Verdugo, A. Shajan, J. Swails, J. Wang, H. Wei, X. Wu, Y. Wu, S. Zhang, S. Zhao, Q. Zhu, T.E. Cheatham, D.R. Roe, A. Roitberg, C. Simmerling, D.M. York, M.C. Nagan, K.M. Merz, AmberTools, J. Chem. Inf. Model. 63 (2023) 6183–6191, https://doi.org/10.1021/acs.jcim.3c01153.
[45] J.A. Maier, C. Martinez, K. Kasavajhala, L. Wickstrom, K.E. Hauser, C. Simmerling, ff14SB: improving the accuracy of protein side chain and backbone parameters from ff99SB, J. Chem. Theory Comput. 11 (2015) 3696–3713, https://doi.org/10.1021/acs.jctc.5b00255.
[46] R. Galindo-Murillo, J.C. Robertson, M. Zgarbová, J. Šponer, M. Otyepka, P. Jurečka, T.E. Cheatham, Assessing the current state of amber force field modifications for DNA, J. Chem. Theory Comput. 12 (2016) 4114–4127, https://doi.org/10.1021/acs.jctc.6b00186.
[47] W.L. Jorgensen, J. Chandrasekhar, J.D. Madura, R.W. Impey, M.L. Klein, Comparison of simple potential functions for simulating liquid water, J. Chem. Phys. 79 (1983) 926–935, https://doi.org/10.1063/1.445869.
[48] M.R. Machado, S. Pantano, Split the charge difference in two! A rule of thumb for adding proper amounts of ions in MD simulations, J. Chem. Theory Comput. 16 (2020) 1367–1372, https://doi.org/10.1021/acs.jctc.9b00953.
[49] P. Eastman, J. Swails, J.D. Chodera, R.T. McGibbon, Y. Zhao, K.A. Beauchamp, L.-P. Wang, A.C. Simmonett, M.P. Harrigan, C.D. Stern, R.P. Wiewiora, B.R. Brooks, V.S. Pande, OpenMM 7: rapid development of high performance algorithms for molecular dynamics, PLoS Comput. Biol. 13 (2017) e1005659, https://doi.org/10.1371/journal.pcbi.1005659.
[50] D.R. Roe, T.E. Cheatham, PTRAJ and CPPTRAJ: software for processing and analysis of molecular dynamics trajectory data, J. Chem. Theory Comput. 9 (2013) 3084–3095, https://doi.org/10.1021/ct400341p.
[51] W. Humphrey, A. Dalke, K. Schulten, VMD: visual molecular dynamics, J. Mol. Graph. 14 (33–38) (1996) 27–28, https://doi.org/10.1016/0263-7855(96)00018-5.
[52] L. Monticelli, S.K. Kandasamy, X. Periole, R.G. Larson, D.P. Tieleman, S.-J. Marrink, The MARTINI coarse-grained force field: extension to proteins, J. Chem. Theory Comput. 4 (2008) 819–834, https://doi.org/10.1021/ct700324x.
[53] S.J. Marrink, H.J. Risselada, S. Yefimov, D.P. Tieleman, A.H. de Vries, The MARTINI force field: coarse grained model for biomolecular simulations, J. Phys. Chem. B 111 (2007) 7812–7824, https://doi.org/10.1021/jp071097f.
[54] D.H. de Jong, G. Singh, W.F.D. Bennett, C. Arnarez, T.A. Wassenaar, L.V. Schäfer, X. Periole, D.P. Tieleman, S.J. Marrink, Improved parameters for the Martini coarse-grained protein force field, J. Chem. Theory Comput. 9 (2012) 687–697, https://doi.org/10.1021/ct300646g.
[55] R.P. Joosten, T.A.H. te Beek, E. Krieger, M.L. Hekkelman, R.W.W. Hooft, R. Schneider, C. Sander, G. Vriend, A series of PDB related databases for everyday needs, Nucleic Acids Res. 39 (2010) D411–D419, https://doi.org/10.1093/nar/gkq1105.
[56] W. Kabsch, C. Sander, Dictionary of protein secondary structure: pattern recognition of hydrogen-bonded and geometrical features, Biopolymers 22 (1983) 2577–2637, https://doi.org/10.1002/bip.360221211.
[57] J.J. Uusitalo, H.I. Ingólfsson, P. Akhshi, D.P. Tieleman, S.J. Marrink, Martini coarse-grained force field: extension to DNA, J. Chem. Theory Comput. 11 (2015) 3932–3945, https://doi.org/10.1021/acs.jctc.5b00286.
[58] T.A. Wassenaar, H.I. Ingólfsson, R.A. Böckmann, D.P. Tieleman, S.J. Marrink, Computational lipidomics with insane: a versatile tool for generating custom membranes for molecular simulations, J. Chem. Theory Comput. 11 (2015) 2144–2155, https://doi.org/10.1021/acs.jctc.5b00209.
[59] M.J. Abraham, T. Murtola, R. Schulz, S. Páll, J.C. Smith, B. Hess, E. Lindahl, GROMACS: high performance molecular simulations through multi-level parallelism from laptops to supercomputers, SoftwareX 1–2 (2015) 19–25, https://doi.org/10.1016/j.softx.2015.06.001.
[60] S. Páll, M.J. Abraham, C. Kutzner, B. Hess, E. Lindahl, Tackling exascale software challenges in molecular dynamics simulations with GROMACS, in: Solving Software Challenges for Exascale, Springer International Publishing, 2015, pp. 3–27, https://doi.org/10.1007/978-3-319-15976-8_1.
[61] T.P. Consortium, Promoting transparency and reproducibility in enhanced molecular simulations, Nat. Methods 16 (2019) 670–673, https://doi.org/10.1038/s41592-019-0506-8.
[62] B. Hess, H. Bekker, H.J.C. Berendsen, J.G.E.M. Fraaije, LINCS: a linear constraint solver for molecular simulations, J. Comput. Chem. 18 (1997) 1463–1472, https://doi.org/10.1002/(sici)1096-987x(199709)18:12<1463::aid-jcc4>3.0.co;2-h.
[63] Z. Tothova, A.-L. Valton, R.A. Gorelov, M. Vallurupalli, J.M. Krill-Burger, A. Holmes, C.C. Landers, J.E. Haydu, E. Malolepsza, C. Hartigan, M. Donahue, K. D. Popova, S. Koochaki, S.V. Venev, J. Rivera, E. Chen, K. Lage, M. Schenone, A. D. D'Andrea, S.A. Carr, E.A. Morgan, J. Dekker, B.L. Ebert, Cohesin mutations alter DNA damage repair and chromatin structure and create therapeutic vulnerabilities in MDS/AML, JCI Insight 6 (2021), https://doi.org/10.1172/jci.insight.142149.
[64] L. Benedetti, M. Cereda, L. Monteverde, N. Desai, F.D. Ciccarelli, Synthetic lethal interaction between the tumour suppressor STAG2 and its paralog STAG1, Oncotarget 8 (2017) 37619–37632, https://doi.org/10.18632/oncotarget.16838.
[65] P. van der Lelij, S. Lieb, J. Jude, G. Wutz, C.P. Santos, K. Falkenberg, A. Schlattl, J. Ban, R. Schwentner, T. Hoffmann, H. Kovar, F.X. Real, T. Waldman, M. A. Pearson, N. Kraut, J.-M. Peters, J. Zuber, M. Petronczki, et al., elife 6 (2017), https://doi.org/10.7554/elife.26980.
[66] Y. Li, K.W. Muir, M.W. Bowler, J. Metz, C.H. Haering, D. Panne, Structural basis for Scc3-dependent cohesin recruitment to chromatin, elife 7 (2018), https://doi.org/10.7554/elife.38356.
[67] Y. Sun, X. Xu, W. Zhao, Y. Zhang, K. Chen, Y. Li, X. Wang, M. Zhang, B. Xue, W. Yu, Y. Hou, C. Wang, W. Xie, C. Li, D. Kong, S. Wang, Y. Sun, RAD21 is the core subunit of the cohesin complex involved in directing genome organization, Genome Biol. 24 (2023) 155, https://doi.org/10.1186/s13059-023-02982-1.

1 Supplementary Figures

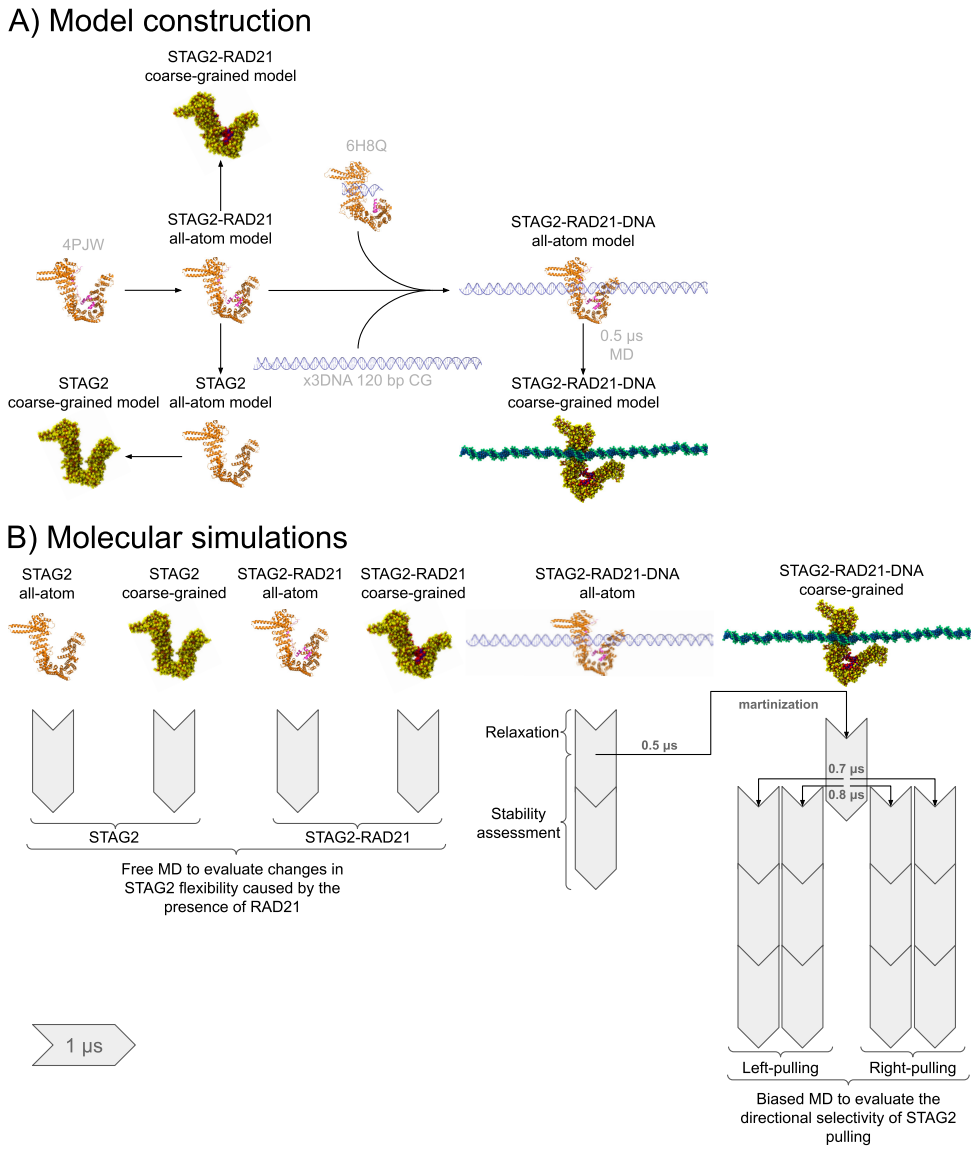

Supplementary Figure 1: Simulation process diagram. **A)** Model construction: Depiction of the steps followed to construct the models used based on: the PDB entries 4PJW and 6H8Q, a 120 bp CG DNA model created by x3DNA, and the 0.5 μs frame obtained from the all-atom STAG2-RAD21-DNA simulation. **B)** Molecular simulations: Visual representation of the simulations performed. The gray arrow blocks indicate 1 μs of MD simulations and are concatenated to illustrate longer simulations (2 μs or 3 μs). On the left, the free MD simulations of the STAG2 and the STAG2-RAD21 complex models are indicated. The purpose of these simulations was to detect differences in the flexibility of STAG2 in presence and absence of RAD21. On the right, the construction of the STAG2-RAD21-DNA coarse-grained model based on the 0.5 μs frame of the MD simulation of the all-atom STAG2-RAD21-DNA model is shown. Additionally, the relaxation of the coarse-grained model, the extraction of the frames at 0.7 μs and 0.8 μs, and the use of these frames to produce left- and right-pulling trajectories are depicted. These pulling trajectories were employed to evaluate whether the displacement of STAG2-RAD21 along the DNA strand is favored in one particular direction.

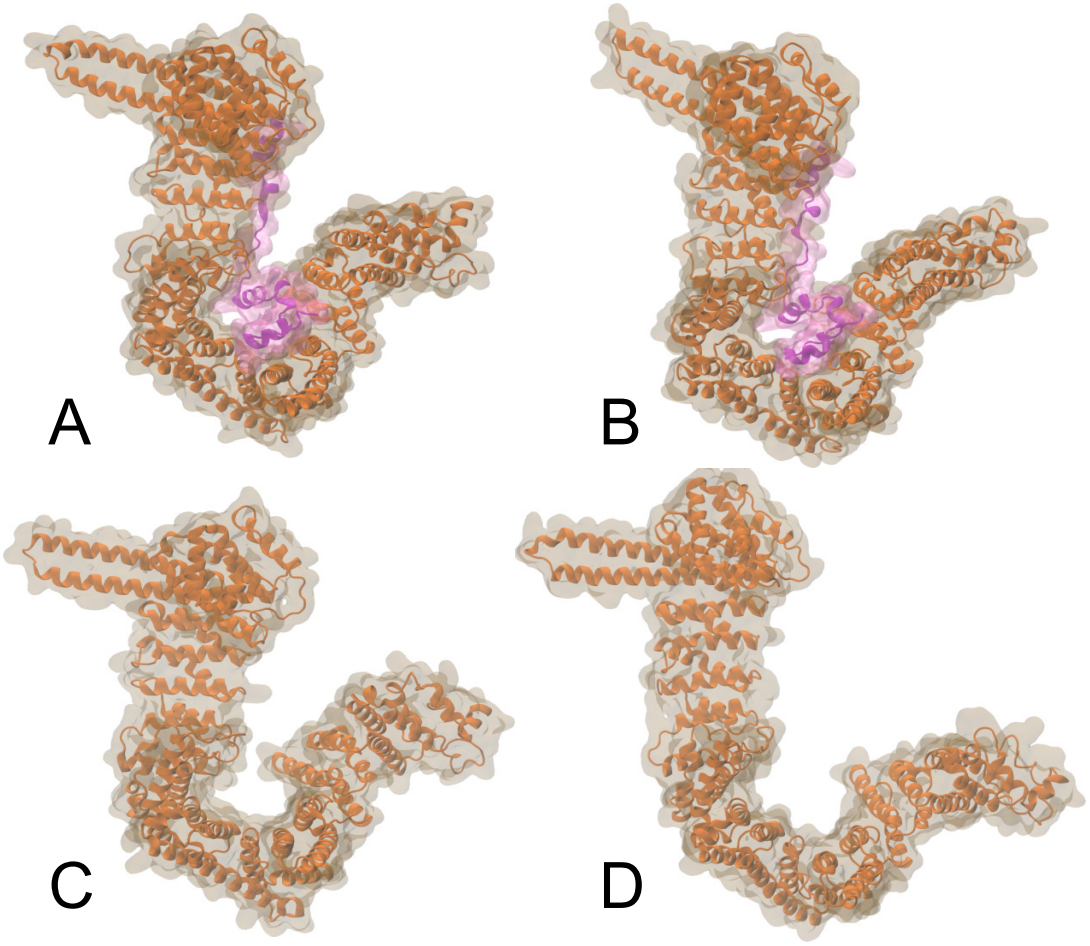

Supplementary Figure 2: Results of the all-atom 1 μs simulations of STAG2 without DNA, to assess the effect of RAD21 (purple) binding on STAG2 (ochre) structure. In the upper section, the initial (**A**) and final (**B**) frames of the simulation of STAG2 in presence of RAD21 are shown. The lower section illustrates the first (**C**) and last (**D**) frames of the simulation in absence of RAD21.

2 Supplementary Tables

Replica	Lefward displacement	Rightward-displacement
Pawl replica 1	1.45 +/- 0.08 nm	0.24 +/- 0.05 nm
Pawl replica 2	1.74 +/- 0.06 nm	0.44 +/- 0.04 nm
Pawl average	1.60 +/- 0.07 nm	0.34 +/- 0.05 nm
Guide replica 1	2.61 +/- 0.04 nm	2.51 +/- 0.09 nm
Guide replica 2	2.38 +/- 0.38 nm	1.95 +/- 0.18 nm
Guide average	2.50 +/- 0.38 nm	2.23 +/- 0.20 nm

Table 1: Mean displacement +/- standard deviation of the STAG2 protein (pawl and guide domains) measured in the last 10 ns of the 3 µs of the simulated leftward or rightward movement.

3 Supplementary Movies

[STAG2_MOVIE_1_LEFTWARD.mp4]

Supplementary Movie 1: Leftward full-turn displacement. Full 3 μs trajectory of the coarse-grained STAG2-RAD21-DNA biased simulation with a 8.75 kcal mol^{-1} Å^{-1} force constant, with the target set to the left, starting from the 800 ns frame of the unbiased simulation.

[STAG2_MOVIE_2_RIGHTWARD.mp4]

Supplementary Movie 2: Rightward locked displacement. Full 3 μs trajectory of the coarse-grained STAG2-RAD21-DNA biased simulation with a 8.75 kcal mol^{-1} Å^{-1} force constant, with the target set to the right, starting from the 800 ns frame of the unbiased simulation.